

# **Exploring the combination of deep-learning based direct segmentation and deformable image registration for cone-beam CT based auto-segmentation for adaptive radiotherapy**

**Xiao Liang, Howard Morgan, Ti Bai, Michael Dohopolski, Dan Nguyen, Steve Jiang\***

Medical Artificial Intelligence and Automation Laboratory and Department of Radiation Oncology, University of Texas Southwestern Medical Center, Dallas, TX, USA

\*Asterisk indicates corresponding author

Corresponding author address:

Steve Jiang

Division of Medical Physics and Engineering

Department of Radiation Oncology

UT Southwestern Medical Center, Dallas, TX

2280 Inwood Road, Dallas, TX 75390

Phone: 214-648-8510

Email: [steve.jiang@utsouthwestern.edu](mailto:steve.jiang@utsouthwestern.edu)

## Abstract

**Purpose:** CBCT-based online adaptive radiotherapy (ART) calls for accurate auto-segmentation models to reduce the time cost for physicians to edit contours, since the patient is immobilized on the treatment table waiting for treatment to start. However, auto-segmentation of CBCT images is a difficult task, majorly due to low image quality and lack of true labels for training a deep learning (DL) model. Meanwhile CBCT auto-segmentation in ART is a unique task compared to other segmentation problems, where manual contours on planning CT (pCT) are available.

**Methods:** To make use of this prior knowledge, we propose to combine deformable image registration (DIR) and direct segmentation (DS) on CBCT for head and neck patients. First, we use deformed pCT contours derived from multiple DIR methods between pCT and CBCT as pseudo labels for training. Second, we use deformed pCT contours as bounding box to constrain the region of interest for DS. Meanwhile deformed pCT contours are used as pseudo labels for training, but are generated from different DIR algorithms from bounding box. Third, we fine-tune the model with bounding box on true labels. We try to compete against DIR-only auto-segmentation.

**Results:** We found that DS on CBCT trained with pseudo labels and without utilizing any prior knowledge for training has very poor segmentation performance compared to DIR-only segmentation. However, adding deformed pCT contours as bounding box in the DS network can dramatically improve segmentation performance, comparable to DIR-only segmentation. The DS model with bounding box can be further improved by fine-tuning it with some real labels instead of using pseudo labels for training. Experiments showed that 7 out of 19 structures have at least 0.2 dice similarity coefficient increase compared to DIR-only segmentation.

**Conclusion:** Utilizing deformed pCT contours as pseudo labels for training and as bounding box for shape and location feature extraction in a DS model is a good way to combine DIR and DS.

**Keywords:** CBCT segmentation, deformable image registration, direct segmentation

## 1. Introduction

Online adaptive radiotherapy (ART) is an advanced radiotherapy technology in which the daily treatment plan is adapted to the patient's changing anatomy (e.g., shrinking tumor, fluctuations in body weight), typically using cone beam computed tomography (CBCT) images. The online nature of the treatment demands high efficiency since the patient is immobilized to the treatment position while waiting for treatment to start. The time-consuming process of segmenting the tumor volumes and organs at risk (OARs) has become a major bottleneck for the widespread use of online ART, warranting an urgent need for accurate auto-segmentation tools (Glide-Hurst et al., 2021).

Auto-segmentation of CBCT images is a very challenging task, mainly due to low image quality and lack of training labels for deep learning (DL) based methods. First, the greater presence of noise and artifacts on CBCT images, such as capping, cupping, ring, and streaking artifacts, makes CBCT more difficult than CT for auto-segmentation task (Lechuga and Weidlich, 2016). Second, the typical application of CBCT in radiotherapy for patient setup causes the lack of manual contours on CBCT images. Therefore limited amount of training labels makes direct auto-segmentation with deep learning methods on CBCT images almost impossible to achieve any high quality segmentation results. Lots of studies have shown that DL-

based direct segmentation (DS) without any help of prior knowledge outputs poor segmentation results (Alam et al., 2021; Beekman et al.; Dahiya et al., 2021; Dai et al., 2021; Léger et al., 2020).

However, auto-segmentation on CBCT for ART is a unique task, where planning CT (pCT) with manual contours are available. With utilization of pCT with manual contours as prior knowledge, some studies have shown that DL-based DS could achieve better results. A simple way to take advantage of pCT and its contours is to directly mix them into limited CBCT training dataset. This cross-domain augmentation of the training set was effective for CBCT augmentation (Léger et al., 2020). With more complicated data augmentation strategy, one study generated variant synthetic CBCT (sCBCT) images with one pair of pCT and CBCT of the same patient, where the generated data is used to train a CBCT segmentation model (Dahiya et al., 2021). Similarly, some other studies utilized artifact induction to convert pCT to sCBCT to make use of high quality CT manual contours for CBCT segmentation (Alam et al., 2021; Schreier et al., 2020).

All the studies mentioned above use data augmentation methods to mitigate lack of training labels on CBCT either by adding pCT with manual contours into training set directly or by generating sCBCT with contour labels from pCT with manual contours. While auto-segmentation results can be improved in some degree by data augmentation, however, the biggest drawback of this type of method is neither CT nor sCBCT can truly represent real CBCT image. Therefore a more robust and popular way to utilize pCT and its high quality contours for CBCT auto-segmentation is through deformable image registration (DIR) methods. By deforming pCT to CBCT's anatomy, pCT contours can be warped accordingly to generate contours on CBCT. Traditional DIR methods including B-spline and Demons algorithms (Fedorov et al., 2012; Gu et al., 2009; Klein et al., 2010) are computationally intensive and time costly, and DL based DIR methods usually requires lots of training data (Han et al., 2021). Thus we developed a new DIR method called test-time optimization in our previous work (Liang et al., 2022). This method only needs one pair of pCT and CBCT images for training, can improve DL-based DIR accuracy, and are time efficient. The biggest benefit of DIR-based segmentation is that topological consistency of contours is preserved by smoothly deforming pCT contours, since most organs have small anatomical changes. But this characteristic also brings the biggest issue when anatomical changes are big, that is DIR-based contour predictions may be quite biased to the shape of CT contours.

However, DL-based DS models that treat segmentation task as a classification problem doesn't have the ability to guarantee shape consistency, therefore doesn't have this issue. Plus, the number of degrees of freedom is much smaller in classification compared to registration, which makes it easier to learn. Combination of both DS and DIR potentially leverages the advantages of both methods. One way to do so is to firstly use a DL-based model to direct segment easier OARs in CBCT images, subsequently uses the segmentation results to constrain the DIR between pCT and CBCT, and finally propagate the target and rest of OARs from pCT to CBCT shown in Figure 1(a) (Archambault et al., 2020). Another way to combine DS and DIR is through joint learning. Joint learning of segmentation and registration has been proposed in deep learning approaches. Typical DL approaches for joint segmentation and registration is shown in Figure 1(b), where input includes only images without any segmentation and the models predict segmentation on both moving and fix images (Estienne et al., 2019; Xu and Niethammer, 2019). Another DL approach for joint learning shown in Figure 1(c) is more similar to our CBCT segmentation task, where moving image, fix image, and moving segmentation are known, and the models predict segmentation on fix image only (Beekman et al., 2021). In DL approaches for joint learning, DS and DIR are combined either through parameter sharing between segmentation model and registration model, or through joint loss

function. However, all those approaches need lots of segmentation labels on fix image for training. However, manual segmentation on CBCT is not common in reality. Another issue we noticed is that there is no joint model performing better than DIR-only model for CBCT segmentation so far (Beekman et al., 2021).

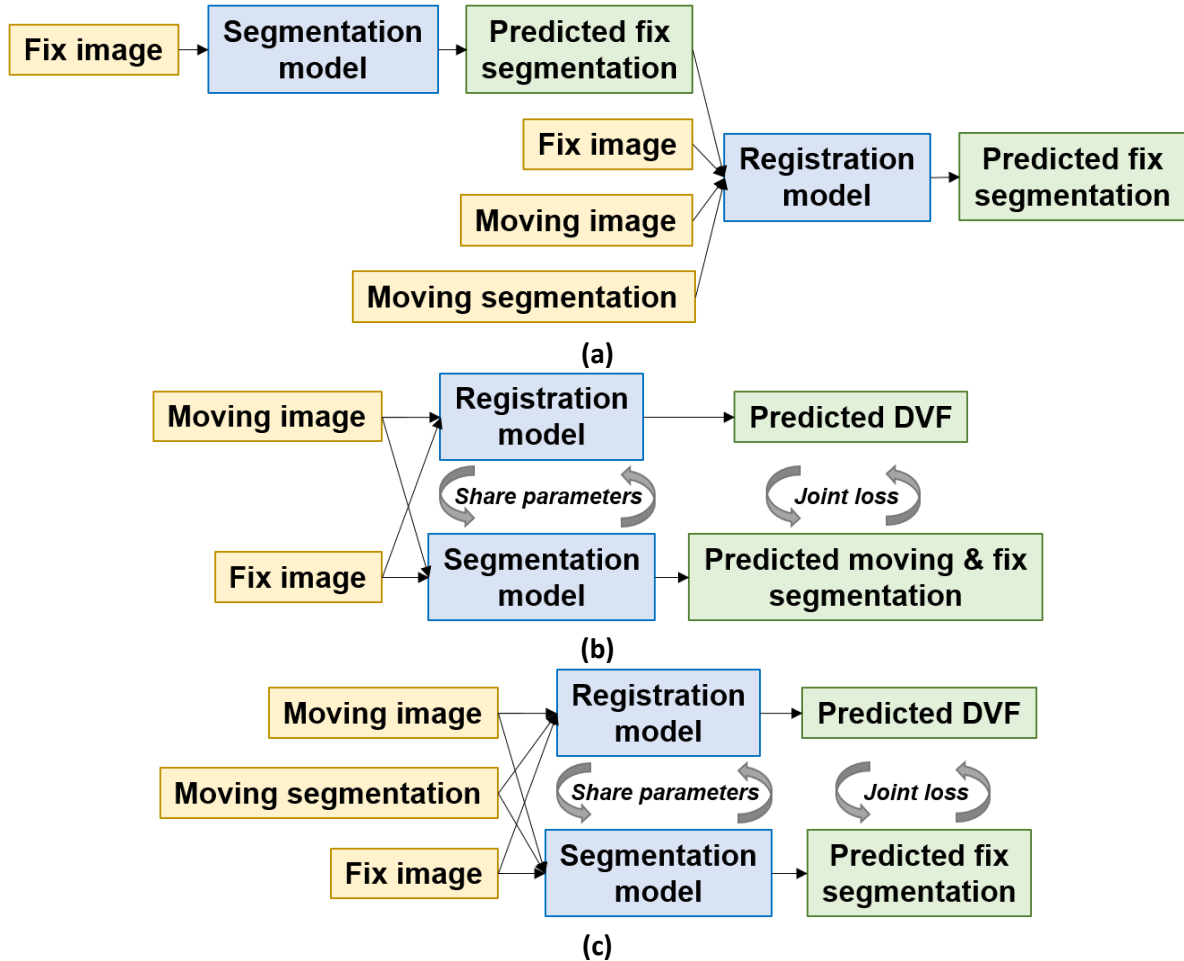


Figure 1. General ways to combine DIR and DS for CBCT segmentation.

In this paper, we explored new ways to combine DS and DIR for CBCT segmentation if only few or even no CBCT manual segmentation labels are available for training. Meanwhile we try to compete with DIR-only CBCT segmentation. In the scenario of no CBCT manual labels available, we propose to use pseudo labels for training, where the pseudo labels are deformed pCT contours. To help localize OARs and target, we propose to add deformed pCT contours as additional channels of the segmentation model. If some manual segmentation on CBCT are available, we can even further improve the model's performance by fine-tuning the model with true labels.

## 2. Methods

### 2.1. Problem definition

In a fully supervised segmentation task, we can denote the training set as  $\mathcal{D} = \{(X, Y)\}^D$ , where  $X \in \mathbb{R}^\Omega$  denotes training images and  $Y \in \{0, 1\}^\Omega$  denotes their corresponding pixel-wise labels.  $\Omega$  denotes its

corresponding spatial domain. Given the labeled dataset  $X = \{x\}$  and  $Y = \{y\}$ , segmentation task intends to learn a function  $F$  with parameter  $\theta$ , which maps the input image  $X$  to the segmentation  $Y$  by minimize the standard Dice loss:

$$\min_{\theta} \mathcal{L}_{Dice}(\theta) := 1 - \frac{[2 \sum_{p \in \Omega} y(p) s_{\theta}(p)] + c}{\sum_{p \in \Omega} y(p) + \sum_{p \in \Omega} s_{\theta}(p) + c}, \quad (1)$$

where  $s_{\theta} = F(x|\theta)$  is the predicted probabilities by the CNNs.  $c$  is a small constant added to prevent divide by 0.  $s_{\theta} \in [0,1]^{\Omega}$  with 0 and 1 denoting background and foreground.

## 2.2. Pseudo label learning

However, CBCT segmentation labels are not always available in the clinic. In the settings of no labeled data available, we can generate pseudo labels for training to leverage from the unlabeled data. To make use of unlabeled data, pseudo labels are used to train the segmentation model. To generate pseudo labels, we firstly deform pCT to its paired CBCT's anatomy to get deformation vector field (DVF). Then we use DVF to warp pCT's contours to get deformed contours. The deformed contours are pseudo labels of CBCT. To address the pseudo label noise, we applied multiple DIR algorithms to pCT and CBCT to generate multiple sets of pseudo labels. By randomly selecting one type of pseudo labels during each training iteration, we could mitigate random errors coming from DIR algorithms. We applied three different DL-based DIR algorithms: FAIM (Kuang and Schmah, 2019), 5-cascaded Voxelmorph (Dalca et al., 2019), and 10-cascaded VTN (Zhao et al., 2019) to generate pseudo labels  $y_1, y_2,$  and  $y_3$  respectively. Now given the dataset  $\mathcal{D} = \{(X, Y)\}^D$ , where  $X = \{x\}$  represents image and  $Y = \{y_i\}$  represents pseudo labels, the segmentation model intends to learn a function  $F$  with parameter  $\theta_p$  formulated similarly to Equation 1:

$$\min_{\theta_p} \mathcal{L}_{Dice}(\theta_p) := 1 - \frac{[2 \sum_{p \in \Omega} y_i(p) s_{\theta_p}(p)] + c}{\sum_{p \in \Omega} y_i(p) + \sum_{p \in \Omega} s_{\theta_p}(p) + c}, \quad (2)$$

where  $s_{\theta_p} = F(x|\theta_p)$  is the model prediction and  $i \in \{1,2,3\}$ .

## 2.3. Bounding box

Another issue with CBCT segmentation is that low image quality causes the direct segmentation model having poor accuracy. To solve this problem, we propose to add bounding box as additional channels of the input, shown in Figure 2. The architecture used in this experiment is a typical U-Net architecture. Besides CBCT image, deformed pCT contours can be used as additional input channels to constrain the region of interest for segmentation. The bounding box serves as shape and location feature extraction. The shape and location features are independently extracted from the bounding box for each level and are combined to features extracted from CBCT images by multiplication. The combined features are further concatenated with the features from the up-sampling layers. The output is multi-organ segmentation masks derived from learned relations between the CBCT images and the bounding box.

However, deformed pCT contours are also used as pseudo labels for training when CBCT true labels are not available. To avoid using the same deformed pCT contours as input and pseudo labels at the same time, we propose to assign two different deformed pCT contours to input and pseudo labels by randomly picking two DIR methods to generate different deformed contours during each training iteration. In this case, input is  $X = \{x, y_j\}$  and label is  $Y = \{y_i\}$ , where  $i, j \in \{1,2,3\}$  and  $i \neq j$ . We could formulate the loss function as the similar style of Equation 1 or Equation 2:

$$\min_{\theta_b} \mathcal{L}_{Dice}(\theta_b) := 1 - \frac{[2 \sum_{p \in \Omega} y_i(p) s_{\theta_b}(p)] + c}{\sum_{p \in \Omega} y_i(p) + \sum_{p \in \Omega} s_{\theta_b}(p) + c}, \quad (3)$$

where  $s_{\theta_b} = F(x, y_j | \theta_b)$  is the model prediction with image  $x$  and deformed pCT segmentation  $y_j$  as input.

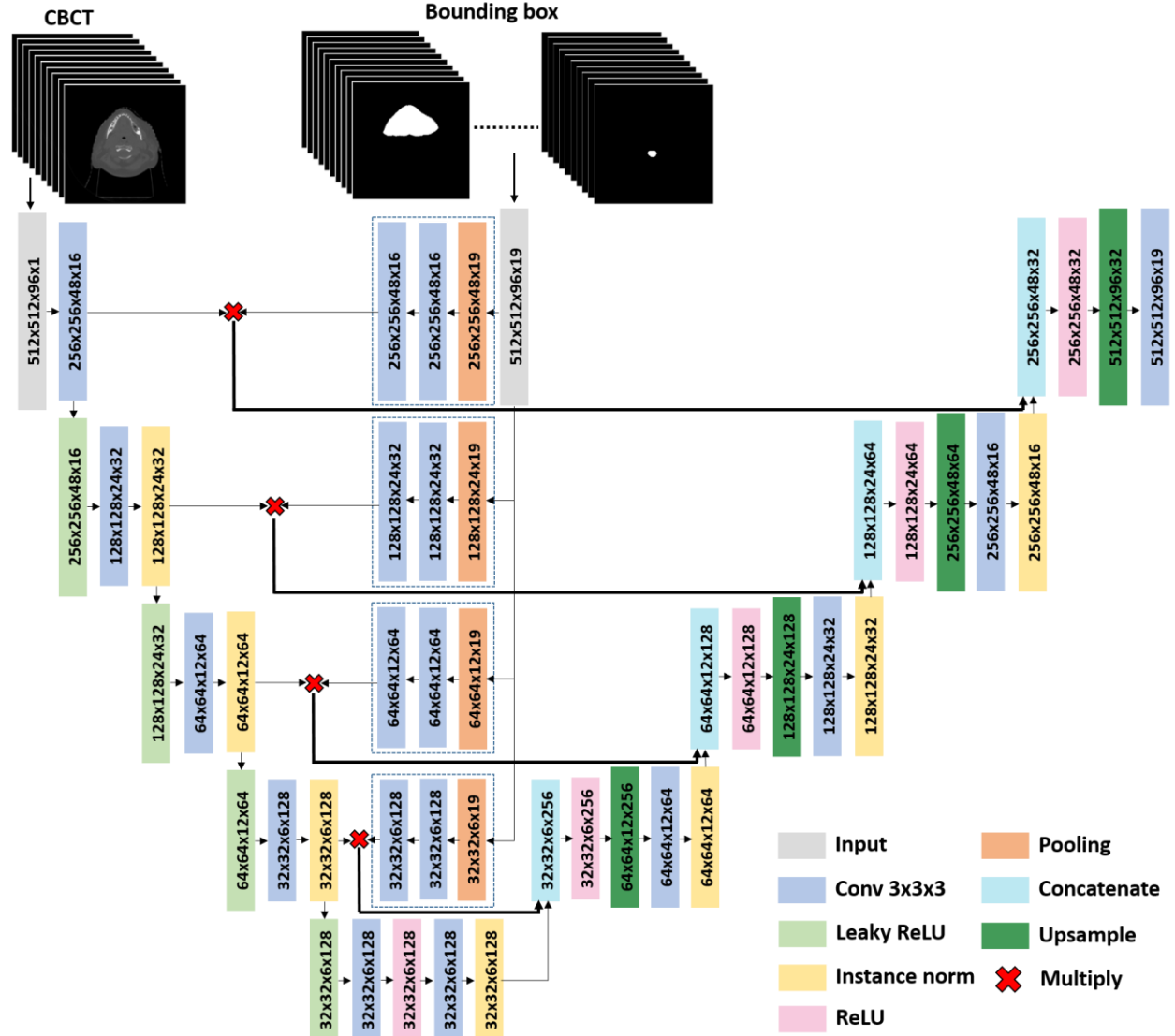


Figure 2. A U-Net architecture with deformed pCT contours as bounding box for CBCT segmentation.

## 2.4. True label fine-tuning

In section 2.3, all the training labels come from generated pseudo labels, assuming that true labels are not available. However, pseudo labels are not equal to true labels. For model trained on the pseudo labels, the error would exist in the trained model. Therefore, if some true labels are available, we propose to further improve the auto-segmentation model accuracy by fine-tuning the trained model from section 2.3 with true labels.

## 2.5. Data

We retrospectively collected data from 137 patients with head and neck (H&N) squamous cell carcinoma treated with conventionally fractionated external beam radiotherapy to a total dose of approximately 70Gy. Each patient’s data included a 3D pCT volume acquired before the treatment course, OARs and target segmentations delineated by physicians on the pCT, and a set of 3D CBCT. The pCT volumes were acquired by a Philips CT scanner with  $1.17 \times 1.17 \times 3.00 \text{ mm}^3$  voxel spacing. The CBCT volumes were acquired by Varian On-Board Imagers with  $0.51 \times 0.51 \times 1.99 \text{ mm}^3$  voxel spacing and  $512 \times 512 \times 93$  dimensions. Among those 137 patients, 39 patients have true segmentation labels on CBCT drawn by a radiation oncology expert. 19 structures that were either critical OARs or had large anatomical changes during radiotherapy courses were selected as segmentation target. These structures were: left brachial plexus (L\_BP), right brachial plexus (R\_BP), brainstem, oral cavity, constrictor, esophagus, nodal gross tumor volume (nGTV), larynx, mandible, left masseter (L\_Masseter), right masseter (R\_Masseter), posterior arytenoid-cricoid space (PACS), left parotid gland (L\_PG), right parotid gland (R\_PG), left superficial parotid gland (L\_Sup\_PG), right superficial parotid gland (R\_Sup\_PG), left submandibular gland (L\_SMG), right submandibular gland (R\_SMG), and spinal cord.

To generate pseudo labels and bounding box, image registration was performed between pCT and CBCT of the 98 patients without true CBCT segmentation labels. pCT is first rigid registered to its corresponding CBCT through Velocity (Varian Inc., Palo Alto, USA), and then deformed registered to the CBCT through our previously proposed DIR methods (Liang et al., 2022): applying test-time-optimization to three different state-of-the-art DIR models including FAIM, 5-cascaded Voxelmorph, and 10-cascaded VTN. Then the pCT contours were warped accordingly to generate deformed pCT contours as pseudo labels or bounding box for training. The rest 39 patients with true CBCT labels were divided to 30 for fine-tuning and 9 for testing. CBCT images and contour masks were padded to size of  $512 \times 512 \times 96$  and  $512 \times 512 \times 96 \times 19$  from  $512 \times 512 \times 93$  and  $512 \times 512 \times 93 \times 19$ , respectively.

## 2.6. Experiments

Firstly, we trained a U-Net model with the 98 patients by switching training label among three types of pseudo labels without adding any bounding box to see the performance of direct segmentation without any prior knowledge ( $Model_{pseudo}$ ). Then we added bounding box into the U-Net and trained the network with pseudo labels to observe performance gain from adding bounding box ( $Model_{BB}$ ). Both the bounding box and pseudo labels were deformed pCT contours, but coming from different DIR algorithms. Finally, we fine-tuned  $Model_{BB}$  on 30 patients with true labels to further improve segmentation accuracy ( $Model_{finetune}$ ), since pseudo labels may contain systematic errors and cannot represent true labels. During fine-tuning stage, we applied early stopping, layer freezing, and lower learning rate to prevent model overfitting. All the models were tested on 9 patients. Dice similarity coefficient (DSC) was used to evaluate segmentation accuracy. In this paper, DIR-only auto-segmentation is the baseline model since it is the most commonly used method in clinics for auto-segmentation due to its better performance compared to other methods. In the experiments, TTO applied 10-cascaded VTN model was considered state-of-the-art DIR baseline model ( $Model_{DIR}$ ).

## 3. Results

### 3.1. Model trained on pseudo labels without bounding box

$Model_{pseudo}$  has much worse performance than  $Model_{DIR}$  shown in Table 1, which means that models depending on CBCT image only cannot derive reliable segmentation results. Reasons causing failure of DS-only models are listed below from our observation.

Firstly and most importantly, CBCT image itself has lots of artifacts and low soft tissue contrast compared to CT. Like the images shown in Figure 3(a), some organs don't have clear boundary from surrounding organs including brainstem, esophagus, parotid gland, and submandibular gland, which makes it much more difficult to segment. However, those organs usually don't have significant anatomical changes, making deformed pCT contours more accurate.

Secondly, superior and inferior segmentation uncertainty degrades DS model performance significantly. DS model isn't sophisticated enough to cope some geometry information if not provided with guidelines shown in Figure 3(b). For example, a consensus guidelines for CT-based delineation of constrictor (Brouwer et al., 2015) specified that the cranial border was defined as the caudal tip of pterygoid plates, and the caudal border as the lower edge of the cricoid cartilage. However, the  $Model_{pseudo}$  failed to pick up those border information during training, leading to delineation error around the borders.

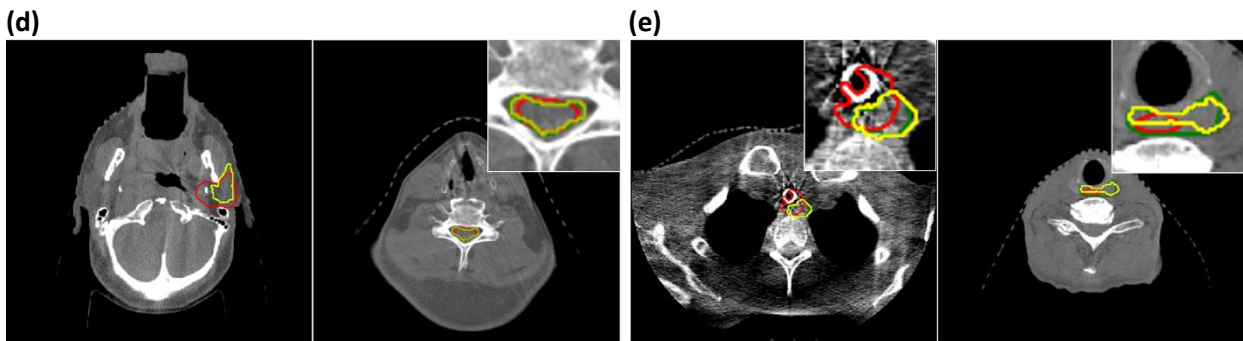
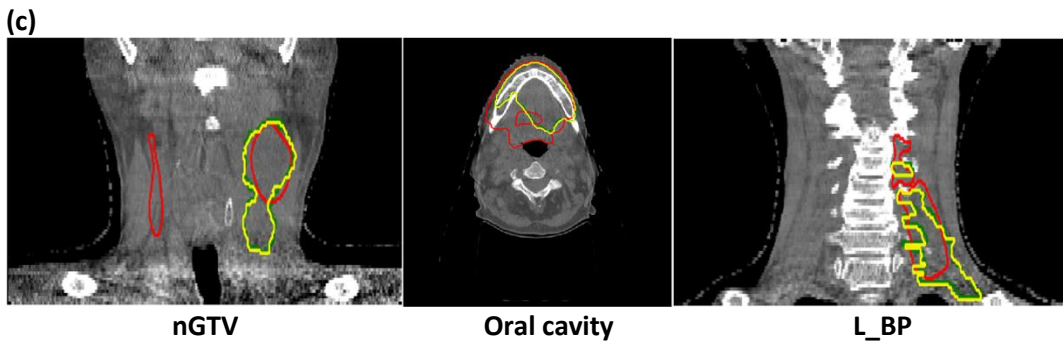
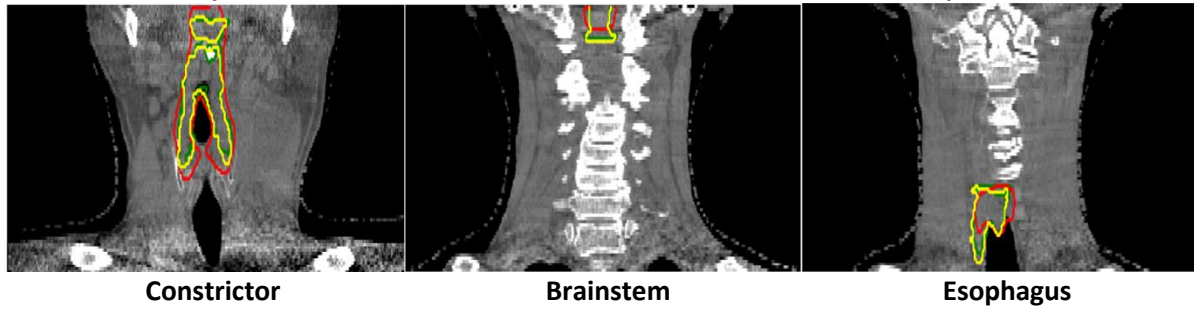
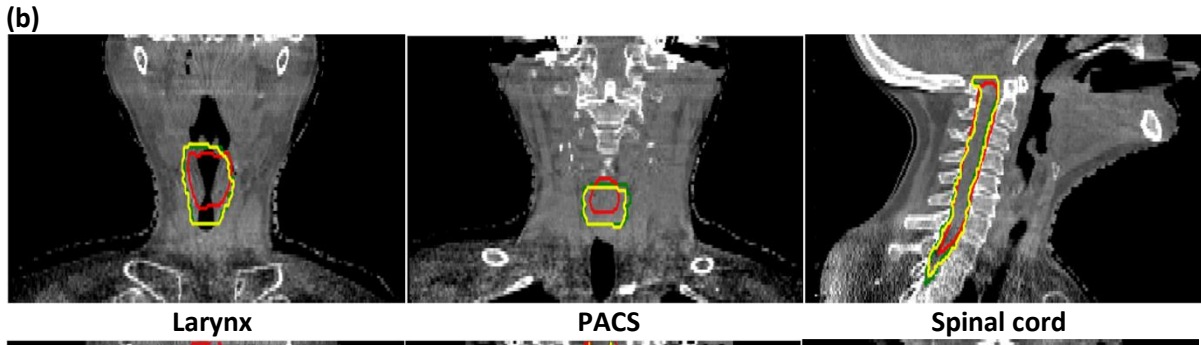
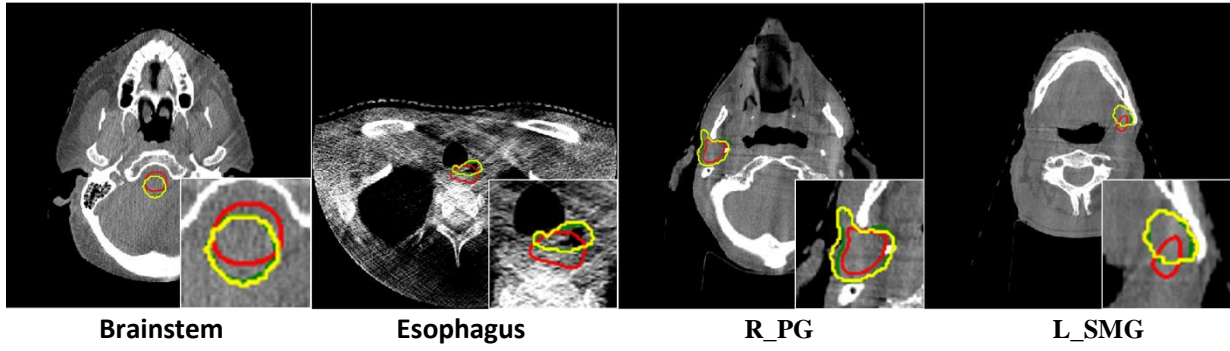
Thirdly, target and some organs are extremely challenging to segment no matter on CT or CBCT. Target delineation like nGTV is more variable and therefore more difficult to predict than organs shown in Figure 3(c). The delineation of oral cavity is often compromised according to its position with target. Brachial plexus is difficult to localize and has step-by-step technique to follow in delineation guidelines. It's not surprising to see DIR-based segmentation prediction has fairly good performance, since it has pCT contours as a start point. However, DS for those extremely difficult structures are easy to fail.

Fourthly, wrong or incomplete labels interfere with DS training. Manual labels sometimes contain misleading information. For example, in Figure 3(d), the manual contour is actually left superficial parotid gland and spinal canal, but mislabeled as parotid gland and spinal cord, separately. We also found that some organs don't have complete delineation in superior-inferior direction from our dataset, because complete delineation is unnecessary if part of the organ is far away from target. However, those wrong or incomplete labels mixed up with right and complete labels can confuse DS model during training.

Fifthly, outliers have some negative impact on model performance during testing phase. Figure 3(e) shows 2 outliers we observed in our dataset. One test patient has a tracheostomy tube in his body, however, no such patients are included in training dataset. The presence of tracheostomy tube leads to wrong delineation of esophagus from DS model. Another test patient has esophagus pushed away to his left side, but no similar patient exists in training dataset.  $Model_{pseudo}$  usually has bad performance on outliers, while  $Model_{DIR}$  is more accurate by preserving the shape information from pCT contours.

(a)





L\_PG

Spinal cord

Esophagus

Esophagus

**Figure 3. Categories that cause poor segmentation performance of DS without any prior knowledge on CBCT.** Green lines are manual contours drawn by a radiation oncology expert, yellow lines are DIR-only derived contours by TTO applied 10-cascaded VTN ( $Model_{DIR}$ ), and red lines come from DS without bounding box ( $Model_{pseudo}$ ).

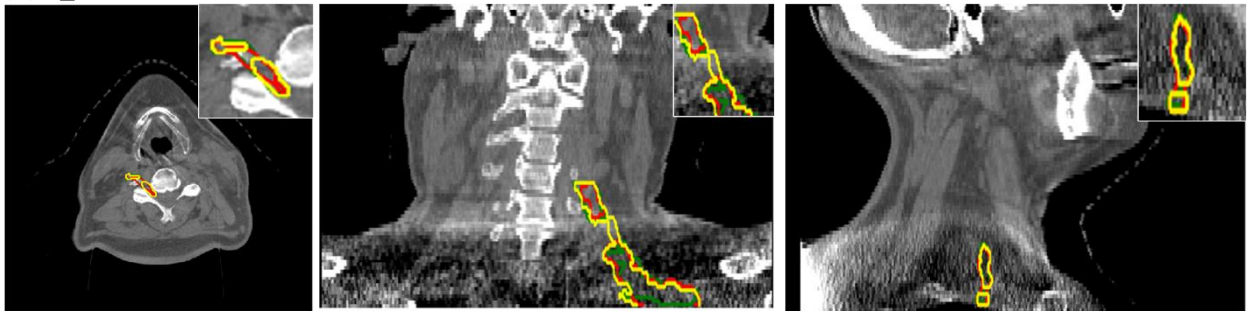
### 3.2. Model trained on pseudo labels with bounding box

Table 1 shows that  $Model_{DIR}$  and  $Model_{BB}$  have similar DSC scores over all 19 structures. Unable to achieve reasonable delineation from DS without prior knowledge, we can significantly improve DS performance comparable to DIR-only segmentation by adding deformed pCT contours as bounding box in the DS model. However,  $Model_{BB}$  cannot surpass  $Model_{DIR}$  since  $Model_{BB}$  preserves the shape of deformed pCT contours including DIR errors.

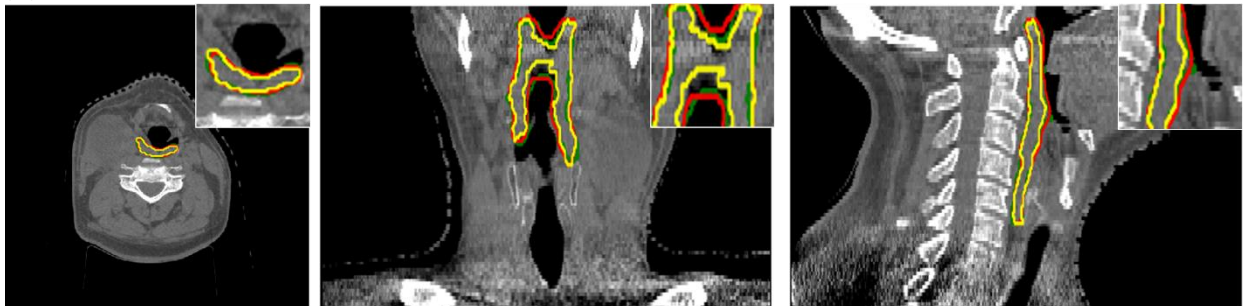
### 3.3 Model fine-tuned on real labels with bounding box

In  $Model_{BB}$ , DIR errors propagates to DS model because pseudo labels are used for training. If  $Model_{BB}$  is further fine-tuned on true labels, biased DIR errors could be corrected. Table 1 shows that DSC scores of  $Model_{finetune}$  are greater than or equal to those of  $Model_{DIR}$  and  $Model_{BB}$ . Taking DIR-only segmentation as baseline,  $Model_{finetune}$  has 7 out of 19 structures that have at least 0.02 DSC improvement. The DSC improvement of a single structure can be up to 0.03. The average DSC over 19 structures by  $Model_{finetune}$  is 0.86 with minimum DSC of 0.72 for L\_BP and maximum DSC of 0.95 for oral cavity. Examples of segmentation from axial, frontal, and sagittal views by  $Model_{DIR}$ ,  $Model_{BB}$ , and  $Model_{finetune}$  are shown in Figure 4 for visual evaluation. We can see that  $Model_{finetune}$  not only can maintain shape characteristics of the prior segmentation, it can also eliminate the errors bought by the prior segmentation.

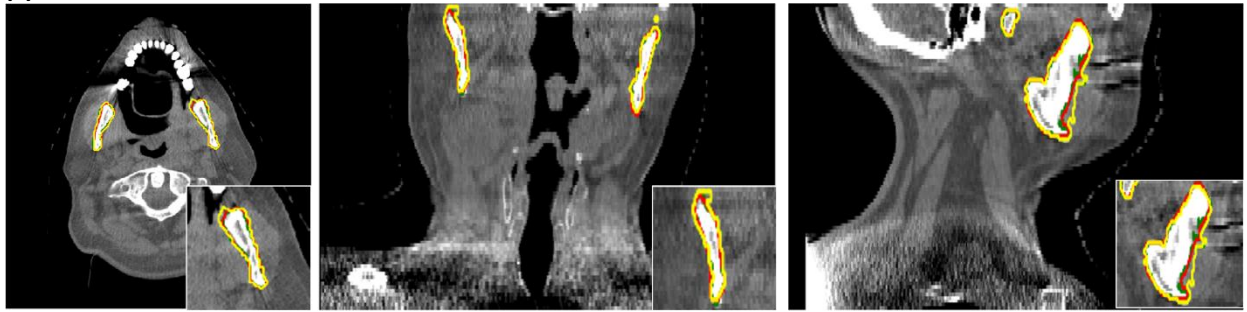
(a) R\_BP



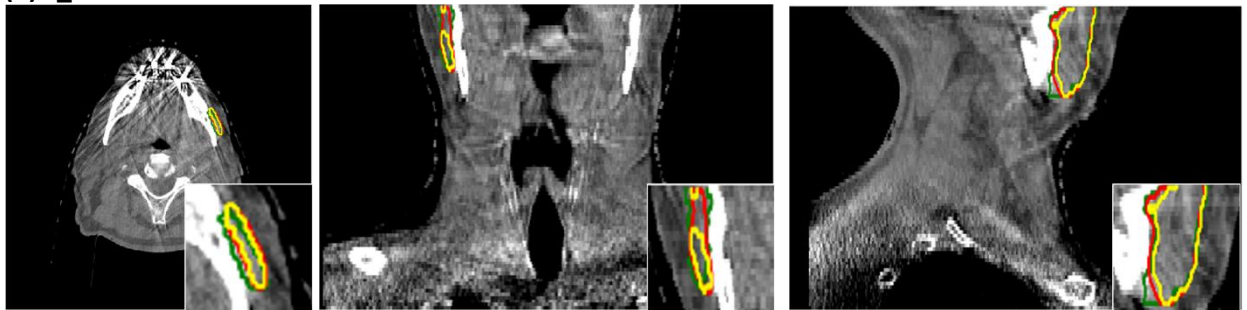
(b) Constrictor



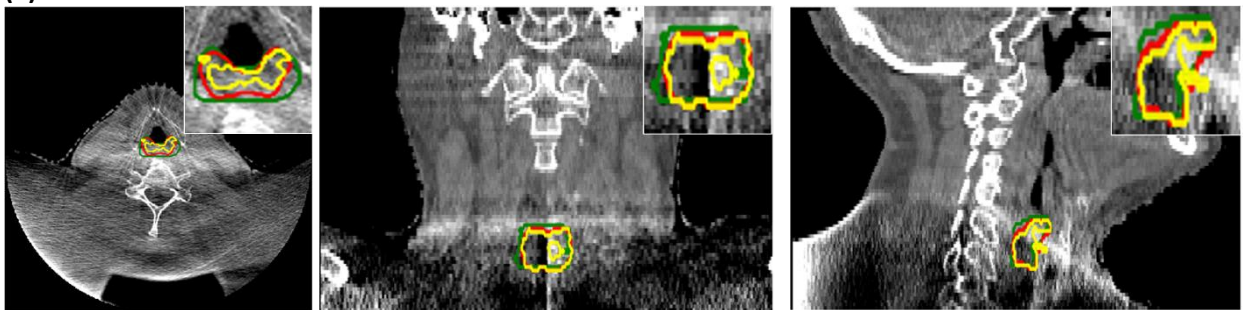
(c) Mandible



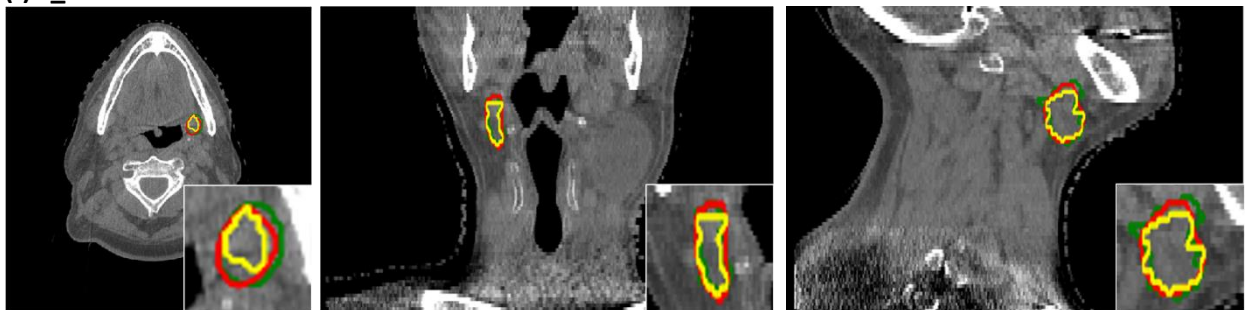
(d) L\_Masseter



(e) PACS



(f) L\_SMG



(g) Spinal cord



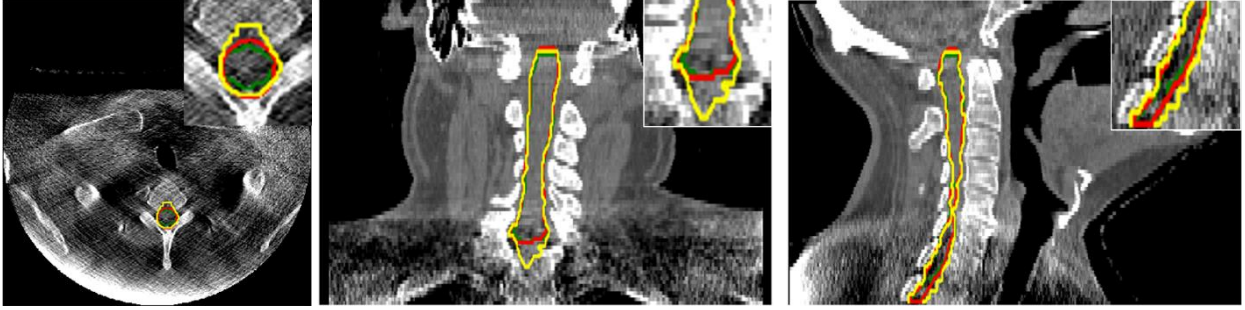


**Figure 4. Segmentation from axial, frontal, and sagittal view.** Green lines are manual contours drawn by a radiation oncology expert, yellow lines are DIR-only derived contours by TTO applied 10-cascaded VTN ( $Model_{DIR}$ ), and red lines come from fine-tuned DS with bounding box ( $Model_{finetune}$ ).

**Table 1. Average DSC of 9 test patients for different auto-segmentation models.**  $Model_{DIR}$  is DIR only segmentation.  $Model_{pseudo}$  is direct DL segmentation using pseudo labels for training.  $Model_{BB}$  is direct DL segmentation with bounding box using pseudo labels for training.  $Model_{finetune}$  is derived from fine-tuning  $Model_{BB}$  with true labels. Numbers in green means DSC has at least 0.02 improvement compared to  $Model_{DIR}$ , while numbers in red means the opposite.

Structure	$Model_{DIR}$	$Model_{pseudo}$	$Model_{BB}$	$Model_{finetune}$
L_BP	0.71	0.34	0.71	0.72
R_BP	0.73	0.40	0.73	0.75
Brainstem	0.91	0.72	0.90	0.91
Oral cavity	0.95	0.60	0.95	0.95
Constrictor	0.83	0.72	0.85	0.86
Esophagus	0.83	0.62	0.83	0.83
nGTV	0.83	0.32	0.84	0.84
Larynx	0.89	0.73	0.89	0.90
Mandible	0.89	0.87	0.90	0.91
L_Masseter	0.90	0.84	0.90	0.92
R_Masseter	0.90	0.83	0.90	0.90
PACS	0.78	0.66	0.79	0.81
L_PG	0.89	0.70	0.88	0.89
R_PG	0.91	0.72	0.90	0.91
L_Sup_PG	0.84	0.60	0.84	0.84
R_Sup_PG	0.86	0.50	0.85	0.86
L_SMG	0.84	0.59	0.85	0.86
R_SMG	0.84	0.55	0.85	0.85
Spinal cord	0.86	0.75	0.86	0.89

#### 4. Discussion and Conclusion:

We believe that auto-segmentation on CBCT without prior knowledge is not an optimal solution due to poor image quality, superior and inferior border uncertainty, delineation complexity, outliers, wrong or incomplete labels, and also lack of true labels. With pCT and its corresponding contours available in ART workflow, we try to make use of pCT contours as prior knowledge for CBCT segmentation by combining DIR and DS to make CBCT auto-segmentation more accurate.

To combine DIR and DS, we propose to use deformed pCT as pseudo labels for training when lack of true labels on CBCT. We also proposed to use deformed pCT as bounding box in the network. By adding bounding box as another channels to constrain shape and localization, DS can be dramatically improved. We found that the DS model with bounding box has comparable but not better performance than DIR-only model if pseudo labels were used for training, mainly because DIR itself persists errors and propagates to DS. To obtain a DS model that can outperform DIR-only segmentation, we found that fine-tuning on true labels is needed.

Fine-tuning with true labels could mitigate DIR errors in DS model. In fine-tuning stage, to prevent overfitting, there are several ways to approach an overfit model (Ying, 2019). Reduce overfitting by training the network on more dataset is not considered in our work since we have limited amount of data with true labels. Reduce overfitting by changing the complexity of the network is one way. In the neural network, the complexity can be reduced by reducing the number of adaptive parameters (Bishop, 1995). For example, the model could be tuned such as via freezing some layers and only updating parameters of the rest layers. Another simple alternative to collecting more data to avoid overfitting is to improve regularization (Goodfellow et al., 2016). One way to improve regularization is early stopping by monitoring model performance on a validation set and stop training when performance degrades. Meanwhile, adding regularization requires smaller learning rate.

In this work, we use H&N patients to test our models, since CBCT-based ART is often used in this site and H&N segmentation is more challenging. After fine-tuning, we found that the DS model surpasses DIR-only model. In conclusion, we propose a new way to combine DIR and DS for CBCT auto-segmentation, that can mitigate the problem of lacking true labels on CBCT and exceed DIR-only segmentation performance.

## **Acknowledgement**

## **Conflict of Interest Statement**

The authors declare no competing financial interest. The authors confirm that all funding sources supporting the work and all institutions or people who contributed to the work, but who do not meet the criteria for authorship, are acknowledged. The authors also confirm that all commercial affiliations, stock ownership, equity interests or patent licensing arrangements that could be considered to pose a financial conflict of interest in connection with the work have been disclosed.

## **Reference**

Alam, S.R., Li, T., Zhang, P., Zhang, S.-Y., Nadeem, S., 2021. Generalizable cone beam CT esophagus segmentation using physics-based data augmentation. *Physics in Medicine & Biology* 66, 065008.  
Archambault, Y., Boylan, C., Bullock, D., Morgas, T., Peltola, J., Ruokokoski, E., Genghi, A., Haas, B., Suhonen, P., Thompson, S., 2020. Making on-line adaptive radiotherapy possible using artificial intelligence and machine learning for efficient daily re-planning. *Med Phys Intl J* 8.  
Beekman, C., van Beek, S., Stam, J., Sonke, J.-J., Remeijer, P., Improving predictive CTV segmentation on CT and CBCT for cervical cancer by diffeomorphic registration of a prior. *Medical Physics* n/a.

Beekman, C., van Beek, S., Stam, J., Sonke, J.-J., Remeijer, P., 2021. Improving predictive CTV segmentation on CT and CBCT for cervical cancer by diffeomorphic registration of a prior. *Medical Physics* n/a.

Bishop, C.M., 1995. *Neural networks for pattern recognition*. Oxford university press.

Brouwer, C.L., Steenbakkens, R.J.H.M., Bourhis, J., Budach, W., Grau, C., Grégoire, V., van Herk, M., Lee, A., Maingon, P., Nutting, C., O'Sullivan, B., Porceddu, S.V., Rosenthal, D.I., Sijtsema, N.M., Langendijk, J.A., 2015. CT-based delineation of organs at risk in the head and neck region: DAHANCA, EORTC, GORTEC, HKNPCSG, NCIC CTG, NCRI, NRG Oncology and TROG consensus guidelines. *Radiotherapy and Oncology* 117, 83-90.

Dahiya, N., Alam, S.R., Zhang, P., Zhang, S.-Y., Li, T., Yezzi, A., Nadeem, S., 2021. Multitask 3D CBCT-to-CT translation and organs-at-risk segmentation using physics-based data augmentation. *Medical Physics* 48, 5130-5141.

Dai, X., Lei, Y., Wang, T., Dhabaan, A.H., McDonald, M., Beitler, J.J., Curran, W.J., Zhou, J., Liu, T., Yang, X., 2021. Head-and-neck organs-at-risk auto-delineation using dual pyramid networks for CBCT-guided adaptive radiotherapy. *Physics in Medicine & Biology* 66, 045021.

Dalca, A.V., Balakrishnan, G., Guttag, J., Sabuncu, M.R., 2019. Unsupervised learning of probabilistic diffeomorphic registration for images and surfaces. *Medical Image Analysis* 57, 226-236.

Estienne, T., Vakalopoulou, M., Christodoulidis, S., Battistella, E., Lerousseau, M., Carre, A., Klausner, G., Sun, R., Robert, C., Mougiakakou, S., Paragios, N., Deutsch, E., 2019. U-ReSNet: Ultimate Coupling of Registration and Segmentation with Deep Nets, *MICCAI 2019: Medical Image Computing and Computer Assisted Intervention – MICCAI 2019*, Shenzhen, China, pp. 310-319.

Fedorov, A., Beichel, R., Kalpathy-Cramer, J., Finet, J., Fillion-Robin, J.-C., Pujol, S., Bauer, C., Jennings, D., Fennessy, F., Sonka, M., Buatti, J., Aylward, S., Miller, J.V., Pieper, S., Kikinis, R., 2012. 3D Slicer as an image computing platform for the Quantitative Imaging Network. *Magnetic Resonance Imaging* 30, 1323-1341.

Glide-Hurst, C.K., Lee, P., Yock, A.D., Olsen, J.R., Cao, M., Siddiqui, F., Parker, W., Doemer, A., Rong, Y., Kishan, A.U., Benedict, S.H., Li, X.A., Erickson, B.A., Sohn, J.W., Xiao, Y., Wuthrick, E., 2021. Adaptive Radiation Therapy (ART) Strategies and Technical Considerations: A State of the ART Review From NRG Oncology. *International Journal of Radiation Oncology\*Biophysics* 109, 1054-1075.

Goodfellow, I., Bengio, Y., Courville, A., 2016. *Deep learning*. MIT press.

Gu, X., Pan, H., Liang, Y., Castillo, R., Yang, D., Choi, D., Castillo, E., Majumdar, A., Guerrero, T., Jiang, S.B., 2009. Implementation and evaluation of various demons deformable image registration algorithms on a GPU. *Physics in Medicine and Biology* 55, 207-219.

Han, X., Hong, J., Reyngold, M., Crane, C., Cuaron, J., Hajj, C., Mann, J., Zinovoy, M., Greer, H., Yorke, E., Mageras, G., Niethammer, M., 2021. Deep-learning-based image registration and automatic segmentation of organs-at-risk in cone-beam CT scans from high-dose radiation treatment of pancreatic cancer. *Medical Physics* 48, 3084-3095.

Klein, S., Staring, M., Murphy, K., Viergever, M.A., Pluim, J.P.W., 2010. *elastix*: A Toolbox for Intensity-Based Medical Image Registration. *IEEE Transactions on Medical Imaging* 29, 196-205.

Kuang, D., Schmah, T., 2019. Faim—a convnet method for unsupervised 3d medical image registration, *International Workshop on Machine Learning in Medical Imaging*. Springer, pp. 646-654.

Lechuga, L., Weidlich, G.A., 2016. Cone Beam CT vs. Fan Beam CT: A Comparison of Image Quality and Dose Delivered Between Two Differing CT Imaging Modalities. *Cureus* 8, e778-e778.

Léger, J., Brion, E., Desbordes, P., De Vleeschouwer, C., Lee, J.A., Macq, B., 2020. Cross-Domain Data Augmentation for Deep-Learning-Based Male Pelvic Organ Segmentation in Cone Beam CT. *Applied Sciences* 10.

Liang, X., Chun, J., Morgan, H., Bai, T., Nguyen, D., Park, J.C., Jiang, S., 2022. Segmentation by Test-Time Optimization (TTO) for CBCT-based Adaptive Radiation Therapy. arXiv preprint arXiv:2202.03978.

Schreier, J., Genghi, A., Laaksonen, H., Morgas, T., Haas, B., 2020. Clinical evaluation of a full-image deep segmentation algorithm for the male pelvis on cone-beam CT and CT. *Radiotherapy and Oncology* 145, 1-6.

Xu, Z., Niethammer, M., 2019. DeepAtlas: Joint Semi-supervised Learning of Image Registration and Segmentation, In: Shen, D., Liu, T., Peters, T.M., Staib, L.H., Essert, C., Zhou, S., Yap, P.-T., Khan, A. (Eds.), *Medical Image Computing and Computer Assisted Intervention – MICCAI 2019*. Springer International Publishing, Cham, pp. 420-429.

Ying, X., 2019. An Overview of Overfitting and its Solutions. *Journal of Physics: Conference Series* 1168, 022022.

Zhao, S., Dong, Y., Chang, E.I., Xu, Y., 2019. Recursive cascaded networks for unsupervised medical image registration, *Proceedings of the IEEE/CVF International Conference on Computer Vision*, pp. 10600-10610.